96/02

Independent Component Analysis Reveals Atypical Electroencephalographic Activity During Visual Perception in Individuals with Autism

Elizabeth Milne, Alison Scope, Olivier Pascalis, David Buckley, and Scott Makeig

Background: Individuals with autistic spectrum disorder (ASD) experience atypical visual perception, yet the etiology of this remains unknown. The aim of this study was to investigate the neural correlates of visual perception in individuals with and without ASD by carrying out a detailed analysis of the dynamic brain processes elicited by perception of a simple visual stimulus.

Methods: We investigated perception in 20 individuals with ASD and 20 control subjects with electroencephalography (EEG). Visual evoked potentials elicited by Gabor patches of varying spatial frequency and stimulus-induced changes in α- and γ-frequency bands of independent components were compared in those with and without ASD.

Results: By decomposing the EEG data into independent components, we identified several processes that contributed to the average event related potential recorded at the scalp. Differences between the ASD and control groups were found only in some of these processes. Specifically, in those components that were in or near the striate or extrastriate cortex, stimulus spatial frequency exerted a smaller effect on induced increases in α- and γ-band power, and time to peak α-band power was reduced, in the participants with ASD. Induced α-band power of components that were in or near the cingulate gyrus was increased in the participants with ASD, and the components that were in or near the parietal cortex did not differ between the two groups.

Conclusions: Atypical processing is evident in individuals with ASD during perception of simple visual stimuli. The implications of these data for existing theories of atypical perception in ASD are discussed.

Key Words: α power, autism, cingulate gyrus, γ power, perception, spatial frequency, visual cortex

In addition to impairments in social behavior and communication, atypical visual perception is also recognized as being part of the autistic spectrum disorder (ASD) phenotype. However, the degree to which visual abnormalities reflect an enhancement or a reduction of perceptual sensitivity is unclear. For example, individuals with ASD respond faster when detecting visual targets than their typically developing counterparts (1,2), yet they show impairment in tasks that involve perceptual integration such as detecting random dot motion in noise (3). This contradiction is mirrored by the weak central coherence account of autism (4) that, on the one hand, suggests superior dis-embedding and, on the other, highlights reduced integration in individuals with ASD.

No model has yet been able to explain parsimoniously both the superior and inferior perceptual skills shown by individuals with ASD, although it has been suggested that "reduced efficiency of neuro-integrative mechanisms" (5; page 2431) might give rise to atypical perception in ASD or that area V1 (primary visual cortex) might be hyper-active in individuals with ASD (6). However, these suggestions have been neither supported nor refuted by experimental evidence, because there have been few attempts to measure the neural correlates of visual perception in individuals with ASD.

The technique of electroencephalography (EEG) is well suited to the investigation of neural integration, because changes in EEG power provide an index of (partial) synchronization of neuronal field potentials. Evoked increases in EEG power are modulated by stimulus characteristics, including spatial frequency (7,8). Gratings of various spatial frequencies therefore provide an idea stimulus with which to investigate perception in ASD.

A recent study compared event related potentials (ERPs) elicited by the onset of low and high spatial frequency gratings in children with ASD and a control group and found reduced ERP amplitude in the participants with ASD (9). However, EEG measured at the scalp is the sum of many electrical processes, including those with neural or muscular origin (for an elegant example see [10], page 106). The far-field potential from each of these sources is recorded, to a greater or lesser degree, by each scalp electrode. This raises the uncomfortable possibility that when comparing EEG response averages between groups there could be many reasons why differences might or might not be found. Independent Component Analysis (ICA) has been successfully applied to EEG data to separate these mixed signals into temporally independent processes, thus providing a more functionally relevant analysis of brain dynamics (11).

Therefore, in the following study we recorded EEG while participants with and without ASD viewed the sudden onset of Gabor patches, the properties of which form a good representation of the profiles of simple cell receptive fields in area V1 (12). We present analysis of the ERP and the changes in α- and γ-band

From the Department of Psychology (EM, AS, OP), The University of Sheffield, Academic Unit of Ophthalmology and Orthoptics (DB), School of Medicine & Biomedical Sciences, Sheffield, United Kingdom; and the Swartz Center for Computational Neuroscience (EM, SM), Institute for Neural Computation, University of California San Diego, La Jolla, California.

Address reprint requests to Elizabeth Milne, Ph.D., Department of Psychology, Western Bank, Sheffield, South Yorkshire, S10 2TN, UK; E-mail: E.Milne@Sheffield.ac.uk.

Received January 23, 2007; revised July 13, 2008; accepted July 24, 2008.

power induced[1] by these stimuli, after applying ICA decomposition to the scalp data.

Methods and Materials

Participants

Twenty children with ASD (2 female) and 20 typically developing (TD) control subjects (2 female) were recruited to this study. All children in the ASD group had received a formal diagnosis of ASD from a child development team within a local clinic. The diagnoses were based on DSM-IV (13) classifications and standardized criteria with the Diagnostic Interview for Social and Communication Disorders (DISCO) (14) and included autism (n = 9), Asperger's syndrome (n = 8), or atypical autism/pervasive developmental disorder–not otherwise specified (n = 3). Two children with ASD had comorbid symptoms of attention-deficit/hyperactivity disorder, and one had Tourette's Syndrome. One child had taken medication (sodium picosulfate) within 24 hours of taking part in the study. The typically developing children were recruited from an e-mail list of volunteers and were screened for any history of developmental disorder. The IQ was measured with the Wechsler Abbreviated Scales of Intelligence (15), and visual acuity was assessed by measuring contrast sensitivity at a range of spatial frequencies (VectorVision, 1991). No participant had contrast sensitivity thresholds that deviated from established norms, and there were no significant differences between the mean contrast sensitivity of the two groups (for further details see Supplement 1). The Childhood Autism Rating Scales (CARS) (16) was used to measure autistic symptomatology, and parents were asked to complete the Social Communication Questionnaire (SCQ) (17). One child was subsequently excluded from the ASD group, because despite having a clinical diagnosis of Asperger's syndrome she failed to reach cut-off for autism on either the CARS or the SCQ. Her matched control participant was also removed from further analysis to maintain equivalence between the experimental and control groups. Further participant information is presented in Table 1. The procedures followed were in accordance with the ethical standards of the South Sheffield National Health Service ethics committee and the Declaration of Helsinki.

Table 1. Mean Age, IQ, CARS, and SCQ Scores

	ASD	TD	t, *p* Values
Chronological Age			
Mean	12y 2m	13y 5m	−1.4, >.1
SD	2y 8m	2y 8m	
Range	8y 4m–18y 0m	8y 3m–18y 3m	
Full-Scale IQ			
Mean	102.2	110.3	−1.6, >.1
SD	16.9	13.3	
Range	65–134	78–129	
Verbal IQ			
Mean	102.3	108.2	<1, >.1
SD	19.5	17.2	
Range	65–136	79–133	
Performance IQ			
Mean	102.2	108.4	−1.3, >.1
SD	16.6	11.0	
Range	70–127	81–124	
CARS Score[a]			
Mean	31.4	N/A	
SD	3.6		
Range	25–39.5		
SCQ Score[b]			
Mean	24.4	N/A	
SD	6.7		
Range	9–34		

CARS, Childhood Autism Rating Scale; SCQ, Social Communication Questionnaire; ASD, autism spectrum disorder; TD, typically developing.

[a]Cut-off for autism is 30.

[b]Cut-off for autism is 22.

Stimuli and Procedure

Gabor patches, illustrated in Figure 1, were created with Matlab 6.5 (The Mathworks, Natick, Massachusetts) and the psychophysics toolbox (18,19). They were presented on a 17-inch monitor, which refreshed at 75 Hz. Stimuli were centrally presented on a grey background (average luminance = 14.4 cd/m2). The space-average luminance of each grating was 16.3 cd/m2, and the Michelson contrast, defined by (Lmax − Lmin)/(Lmax + Lmin), was 68%. The slight difference between the average luminance of the background and the stimuli was not visibly apparent and did not lead to any visible edges around the stimuli. At a viewing distance of 114 cm the patches subtended 6.78° × 6.78° of visual angle. All patches were presented in diagonal (45°) orientation, had a gaussian envelope with SD of .68°, and with spatial frequency modulation of .5, 1, 4, or 8 c/°. An additional stimulus, a grey-scaled image of a zebra was presented. Participants were instructed to respond by pressing a response button with the index finger of their dominant hand as quickly as possible whenever they saw the zebra. This was to ensure that participants paid attention to the screen. There were no group differences in the behavioral responses to the zebra stimuli (Supplement 2).

Each of the four Gabor patches was shown 72 times; the zebra was shown 36 times. The order of stimulus presentation was randomized. Each stimulus remained on screen for 507 msec,

[1]Two terms are frequently used to describe event-related changes in spectral power measured by EEG: induced and evoked. Activity induced by events is activity time-locked to the events but not necessarily phase-locked to them. In contrast, activity evoked by events is phase-locked at a particular latency (relative to the onset of events) across single trials. When activity within a frequency band is phase-locked across trials, it contributes to the ERP; however, this is not true in the case of non–phase-locked activity (i.e., random phase). Therefore in the EEG literature, the term "evoked" has come to be used when spectral change is computed by performing time/frequency analysis on the ERP itself, and the term "induced" is used for time/frequency decomposition of single-trial activity. All of the time/frequency transforms reported in this manuscript were carried out on the single trials, because this reveals both evoked and induced activity. To highlight the use of single-trial rather than ERP time/frequency decomposition, we have used the term "induced" to describe changes in spectral power (relative to baseline) reported here. However, when phase-locking of activity (as measured with inter-trial coherence) is reasonably high—as was the case in the components of clusters 5, 11, 13, and 20—mean energy at the dominant ERP frequency band in single trials is nearly the same as the mean of the single trials (the ERP), indicating that phenomenologically, if not practically, the term "evoked" would have been suitable to describe these cases.

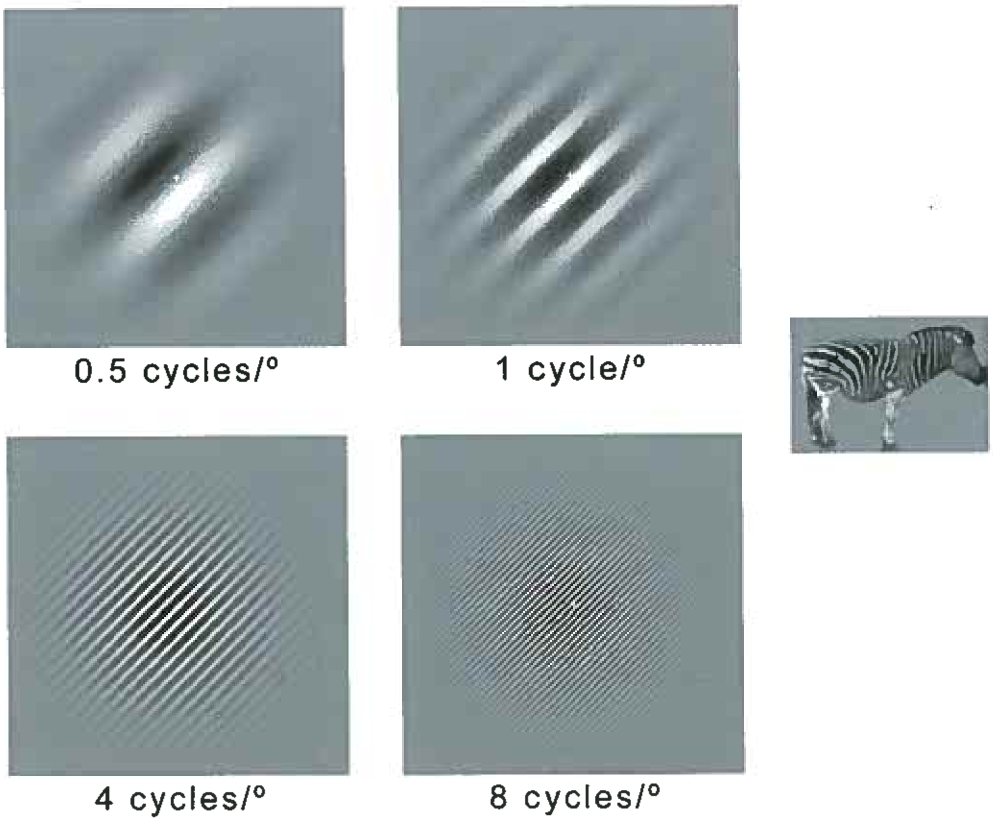

Figure 1. Gabor patches presented at a range of spatial frequencies and the zebra stimulus. The images are to scale but due to printing the Gabor patches are not an accurate representation of spatial frequency.

with an additional variable interstimulus interval of either 312, 507, or 702 msec. A white fixation cross measuring .2° by .2° remained in the center of the screen for the duration of the task. Participants were asked to maintain fixation and to limit their blink frequency during the experiment.

The EEG was continuously recorded with a high-density array of 128 silver-silver chloride electrodes (Electrical Geodesics, Eugene, Oregon) (20). Impedance was kept below 50 KΩ. The signal was amplified (×1000), filtered online with a band-pass of .01–80 Hz, then digitized at a sampling rate of 1 KHz. The electro-oculogram was recorded from bipolar electrode pairs located at the outer canthi and above and below the left and right eyes. Data were analyzed off-line with EEGLAB (21) a freely available open source toolbox (http://www.sccn.ucsd.edu/eeglab) running under Matlab 7.4 (The Mathworks). Data were high-pass filtered (> 1 Hz) and re-referenced to average reference. Continuous data were first screened for any spatially atypical (noisy) time points. The remaining data were decomposed by extended infomax ICA with the algorithm runica (22) as implemented in EEGLAB. The average number of time points decomposed for each subject was 328,484 (5 min, 29 sec) in the TD group and 330,483 (5 min, 31 sec) in the ASD group. An independent samples t test indicated that this was not significantly different [$t(32) < 1$, $p > .1$]. To obtain a stable decomposition, the number of channels entered into the analysis was pruned from 129 to 64 near-evenly spaced channels. Thus, for every participant, ICA returned 64 maximally independent components, each of which is a combination of all 64 channel signals acting as a spatial filter for an independent process or source activity in the scalp data. After running ICA, the data were segmented into epochs of 800 msec (−100–700 msec around stimulus presentation) on the basis of stimulus type (Gabor patches of .5, 1, 4, or 8 c/°) and baseline corrected by subtracting the mean of the 100-ms pre-stimulus interval. Data were screened for artefacts, and epochs containing blink artefacts were rejected. Data from four participants (two with ASD who had comorbid diagnoses of attention-deficit/hyperactivity disorder, and two control subjects) were excluded from further analysis at this stage, because of too few (<75%) artefact-free epochs.

Independent component source locations were estimated by creating an equivalent current dipole model for each component with the dipfit function from EEGLAB that estimates dipole location by applying inverse source modeling methods to a standard boundary element head model (23). Only components whose scalp maps had <15% residual variance from the best-fitting forward model scalp projection were considered for further analysis. Any remaining components that reflected muscle activity, electrocardiogram, or eye movements, on the basis of their dipole location, spectra and scalp maps were considered artefacts and excluded from further analysis. In total, 413 independent components were retained; 229 from the TD group and 184 from the ASD group. The mean numbers of retained components in the TD and ASD groups were 13.5 and 10.8, respectively. An independent-samples t test indicated that these were not significantly different [$t(32) = 1.96$, $p > .05$].

Components were grouped into several clusters with a joint distance measure, on the basis of dipole locations, power

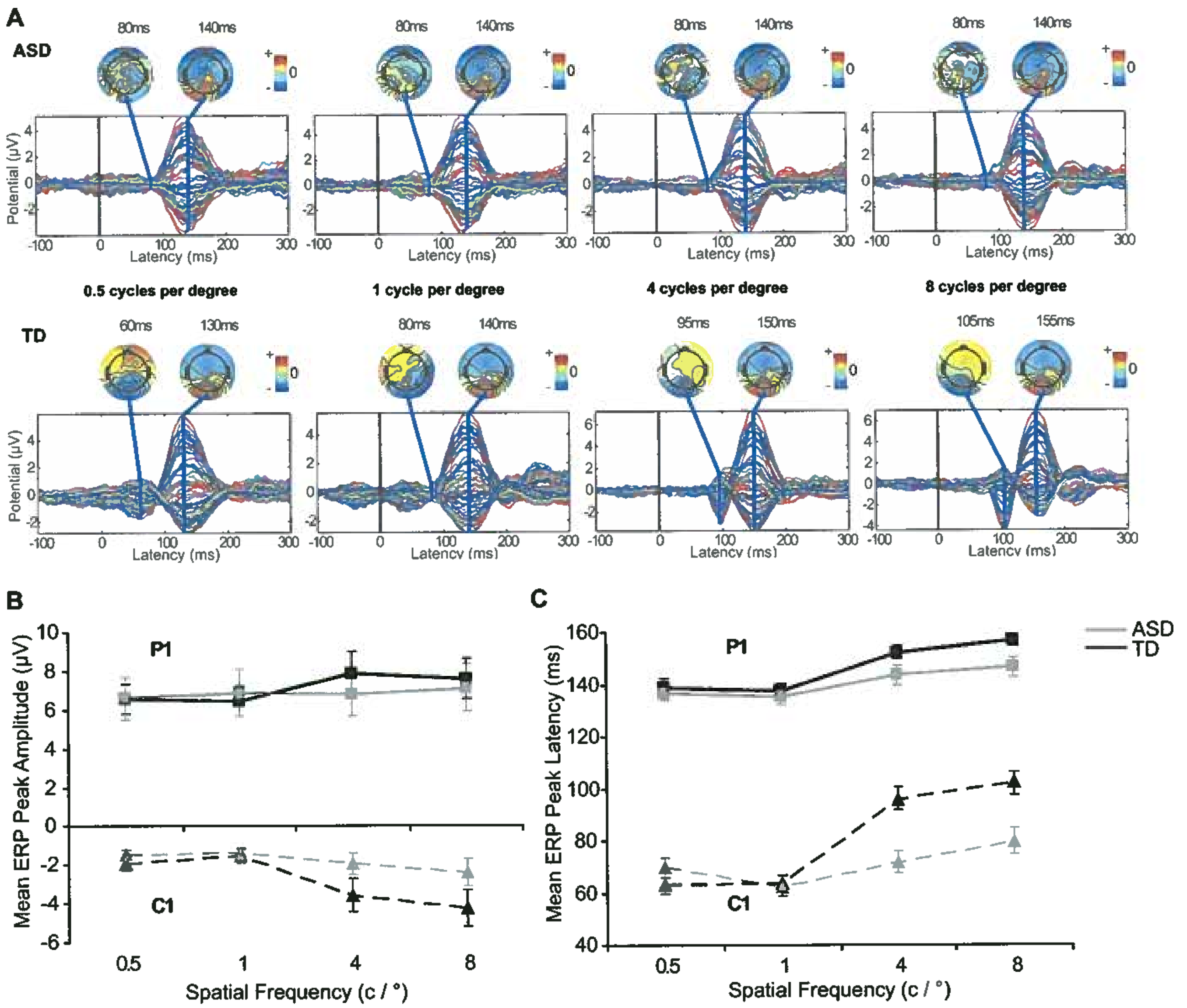

Figure 2. Channel event-related potential (ERP) data. **(A)** Grand average ERP of 64 channels in each group and elicited by each spatial frequency. The ERP is plotted with positive up. The scalp plots show the spatial distribution of group-mean amplitude at specific time points coinciding with the C1 and P1 deflections. **(B and C)** Peak amplitude and the peak latency, respectively, of the C1 and P1 deflections recorded from Oz averaged across participants in each group. Error bars = ± 1 SEM. ASD, autism spectrum disorder; TD, typically developing.

spectra, scalp projections, and mean Event Related Spectral Perturbation (ERSP) and Inter-Trial phase Coherence (ITC) measures. These data from each subject were initially decomposed by Principal Component Analysis (PCA), and the resulting component distances were clustered with a k-means algorithm (for further details of this method see 10).

Results

ERP Channel Data

Figure 2A shows the grand average (within group) ERPs from 64 channels and scalp maps at specified latencies. The first deflection of the ERP, the C1 component, was maximal over the occipital cortex and reached peak between 80 and 100 msec, consistent with previously published data (24). The label "C" rather than "P" (positive) or "N" (negative) is given, because the polarity of this component can vary (25); however, in the majority of experiments C1 is a negative-going deflection (24, 26, 27). The C1 was followed by a positive-going deflection, "P1" that reached peak between 120 and 160 msec. Variables were extracted from each participant by identifying the amplitude and latency of the minimum and maximum points of the ERP within a latency window from 50 to 200 msec. All data were extracted from channel 76 (Electrical Geodesics), which approximates to Oz (central occipital) in the International 10-20 system. These values were then entered into four separate repeated measures analyses of variance (ANOVAs) (in this and all subsequent ANOVAs violations of the assumption of sphericity were corrected for by applying Greenhouse-Geisser correction) with between-subjects factors of group (ASD or TD) and within-

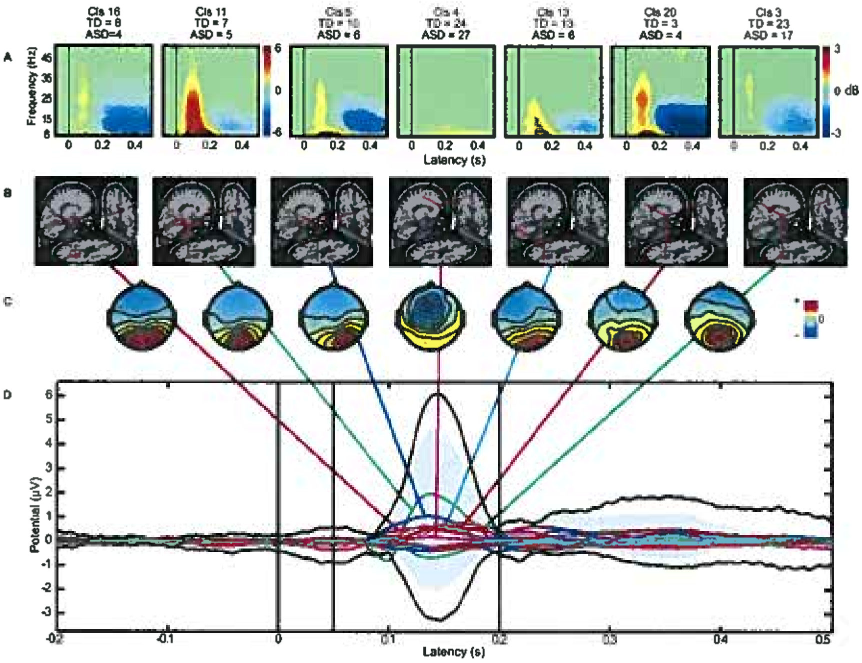

Figure 3. Mean spectrogram **(A)**, dipole **(B)** and scalp map **(C)** of each of the seven component clusters that accounted for most variance in the grand average ERP **(D)**. **(A)**: Mean event related spectral perturbation, changes are relative to the pre-stimulus baseline (NB range–6 to 6 dB in clusters 16 and 11), nonsignificant changes (based on bootstrap statistics with $p < .01$) are masked by green shading. **C:** Weights of the mixing matrix back-projected to a head plot, indicating the relative weights with which the cluster projects to each of the scalp channels. **D:** Black traces, envelope of the maximum and minimum channel values at each latency; colored lines, envelope of the contributions of the clusters to the ERP; blue shading, the summed contribution of these clusters. Abbreviations as in Figure 2.

subjects factors of stimulus spatial frequency (.5, 1, 4, or 8 c/°). Each participant's ERP from channel Oz is illustrated in Supplement 3.

Peak latency of C1 occurred earlier in the ASD group than in the TD group [$F(1,32) = 10.7$, $p < .001$, $\eta_p^2 = .25$]. This main effect interacted with stimulus spatial frequency [$F(2,7,86.2) = 8.8$, $p < .001$, $\eta_p^2 = .21$]. Simple effects analyses indicated that stimulus spatial frequency influenced C1 latency to peak less in the ASD group [$F(2.7,44.2) = 3.2$, $p < .05$, $\eta_p^2 = .17$] than in the TD group [$F(2.5,39.7) = 36.0$, $p < .01$, $\eta_p^2 = .69$]. Independent samples t tests indicated that the group difference was significant when C1 was elicited by the higher spatial frequency stimuli only [4 c/°, $t(32) = 3.88$, $p < .01$, Cohen's d = 1.4, 8 c/°, $t(32) = 3.58$, $p < .01$, Cohen's d = 1.2].

There was a trend toward peak latency of P1 occurring earlier in the ASD than the TD group [$F(1,32) = 3.2$, $p = .08$, $\eta_p^2 = .09$]. This did not interact with spatial frequency.

There was no significant group difference in amplitude of either C1 P1 deflection and no interaction between group and spatial frequency.

Independent Components

Figure 3 shows the scalp maps, mean dipole location, and spectrograms of the seven clusters of components that accounted for the most variance in the scalp EEG between 50 and 200 msec. The estimated Talairach coordinates and the nearest grey matter of the mean equivalent current dipole of each cluster (28) are presented in Table 2.

These seven clusters were divided into three sub-categories: those comprising components that primarily showed stimulus-induced increases in power around 100 msec after stimulus onset (clusters 5, 11, 13, and 20); those comprising components that primarily showed decreases in power approximately 300 msec after stimulus onset (clusters 16 and 3); and cluster 4, which showed a small but significant increase in low α-band power approximately 300 msec after stimulus onset.

Time/frequency transforms were computed in EEGLAB with wavelets with a 3-cycle window centered at 100 msec. In each time/frequency analysis we computed the mean change in power (measured in dB) across single-trial epoch latencies, relative to the pre-stimulus baseline. Values were extracted from

Table 2. Talairach Coordinates and Nearest Grey Matter to the Average Dipole Location of Each of the Seven Clusters of Independent Components

Cluster Number	Talairach Coordinates x	y	z	Lobe	Nearest Grey Matter	BA
16	16	−64	23	R Parietal	Precuneus	31
11	7	−77	25	R Occipital	Cuneus	18
5	34	−61	31	R Temporal	MT (V5)	39
4	−17	−2	46	L Limbic	Cingulate gyrus	24
13	14	−78	−16	R Occipital	Lingual gyrus	18
20	7	−54	45	R Parietal	Precuneus	31
3	5	−59	47	R Parietal	Precuneus	7

This localization is approximate, because not all of the equivalent current dipoles from each independent component in the cluster were located at the site of the mean dipole. Furthermore, the position of the electrodes was co-registered with the Montreal Neurological Institute average (adult) brain. BA, Brodmann area; MT, middle temporal.

the resulting time course for each component from the frequency showing maximum power within the range of 8–13 Hz (α) and 30–40 Hz (γ) within the latency window from 50 to 200 msec for clusters 5, 11, 13, and 20 and from 200 to 400 msec in cluster 4. Dependent variables were the latency and magnitude of the induced power peak relative to baseline in both α and γ frequency bands for each component. These values were entered into separate repeated measures ANOVAs. Clusters 13 and 4 did not show significant post-stimulus changes in γ-band activity; therefore components from these clusters were not included in the γ-band analysis. In the following sections, the components showing early increases in spectral power (clusters 5, 11, 13, and 20) are included in one analysis, and the components of cluster 4 are the subject of a second analysis. There were no group differences in the spectral characteristics of the components in clusters 16 and 3, so this analysis is omitted from the manuscript but presented in Supplement 4.

The α-Band Power Increase and Latency in Clusters 5, 11, 13, and 20

As illustrated in Figure 4A, induced α-band power was higher after presentation of high spatial frequency than low spatial frequency stimuli [$F(1.6,83.9) = 20.6$, $p < .01$, $\eta_p^2 = .28$]. This effect interacted with group [$F(1.6,83.9) = 4$, $p < .05$]. Post hoc analyses indicated that the effect was larger in the TD [$F(1.5,48.6) = 24$, $p < .05$, $\eta_p^2 = .43$] than the ASD group [$F(1.7,34.5) = 3.5$, $p < .05$, $\eta_p^2 = .15$]. Independent samples *t* tests indicated that there were no significant group differences in relative α-band power induced by any of the spatial frequencies.

The α-band power peak occurred later when induced by high spatial frequencies than by low spatial frequencies [$F(2.5,131.2) = 7.4$, $p < .01$, $\eta_p^2 = .12$, see Figure 4B]. There was a marginally significant main effect of group, because peak α-band power occurred earlier in the ASD than the TD group [$F(1,52) = 3.9$, $p = .053$, $\eta_p^2 = .07$]. The latency at which induced α-band power became significantly greater than baseline (on the basis of bootstrap statistics with an α value of $p < .01$) also occurred earlier in the ASD compared with the TD group [$F(1,52) = 4.0$, $p = .05$, $\eta_p^2 = .07$]. There were no significant group × spatial frequency interactions in α-band peak latency.

The γ-Band Power Increase and Latency in Clusters 5, 11, and 20

As shown in Figure 4A, induced increases in γ-band power were significantly larger after presentation of high spatial frequency compared with low spatial frequency stimuli [$F(1.3,41.9) = 16.7$, $p < .01$, $\eta_p^2 = .34$]. The group × spatial frequency interaction approached significance [$F(1.3,41.9) = 3.7$, $p = .054$, $\eta_p^2 = .10$], and simple effects analyses indicated that stimulus spatial frequency-modulated increases in γ-band power were smaller in the ASD than the TD group [TD group: $F(1.2,22.5) = 16.1$, $p < .01$, $\eta_p^2 = .46$; ASD group: $F(1.5,21.5) = 3.7$, $p = .051$, $\eta_p^2 = .21$]. Independent samples *t* tests indicated that there were no significant group differences in relative γ-band power induced by any of the spatial frequencies.

There were no significant group differences in the latency of the γ-band peak.

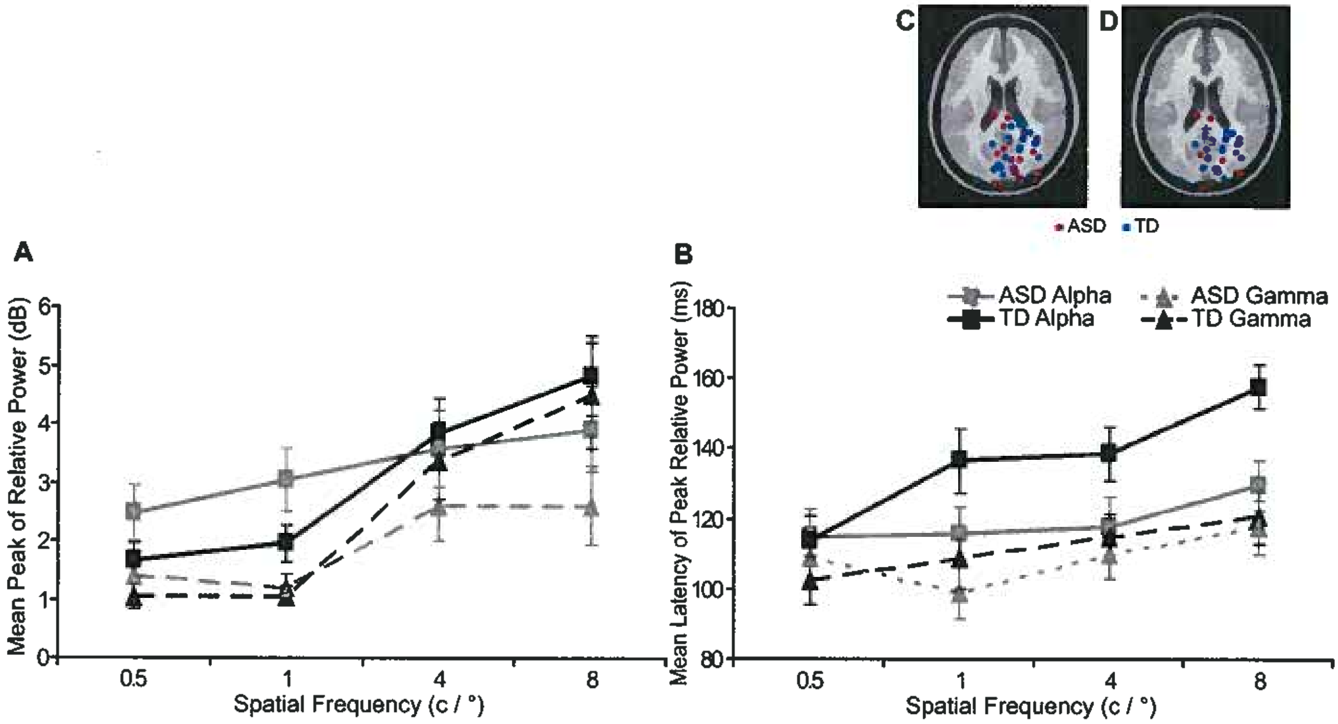

Figure 4. Mean peak increase **(A)** and mean latency of peak increase **(B)** relative to baseline of induced α-band and γ-band power in the components located in or near the striate or extrastriate cortex. **(A)** The mean peak increase relative to the pre-stimulus baseline in α- and γ-band power induced by the four different spatial frequency Gabor patches and for each group separately. **(B)** The mean latency of the peak of the induced increase. Error bars = ± 1 SEM. The α-band power is calculated as the mean of the peak increase of the independent components that contributed to clusters 5, 11, 13, and 20 (the dipole locations of each of these components is plotted in **C**). The γ-band power is calculated as the mean peak increase of the independent components that contributed to clusters 5, 11, and 20 (the dipole locations of each of these components is plotted in **D**). ASD, autism spectrum disorder; TD, typically developing.

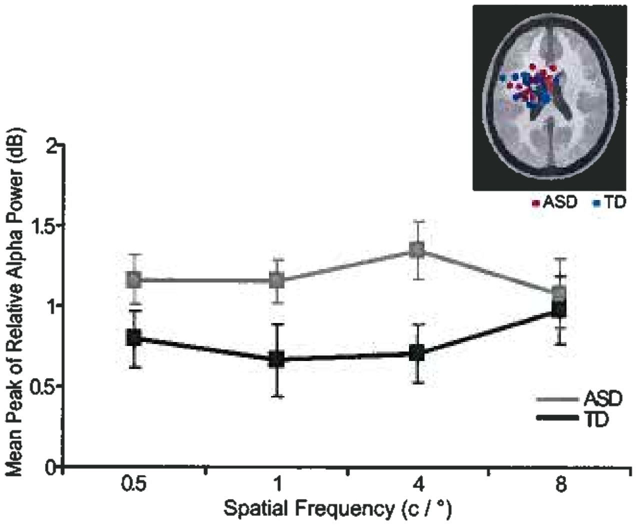

Figure 5. Mean peak increase, relative to baseline, of induced α-band power in the components located in or near left cingulate gyrus. The mean peak increase, relative to the pre-stimulus baseline, in α band power (measured in decibels) of the independent components that contributed to cluster 4. Error bars = ± 1 SEM. ASD, autism spectrum disorder; TD, typically developing.

Low α-Band Power Increase in Cluster 4

The increase in α-band power in the components of cluster 4 was significantly larger in the participants with ASD than in the TD group [$F(1,49) = 5.6$, $p < .05$, $\eta p^2 = .10$, see Figure 5]. No other effects or interactions were significant.

Relationship Between Electrophysiological Data and Participant Characteristics

Correlation coefficients were computed to investigate the relationship between the electrophysiological markers (C1 and P1 amplitude and latency and α-band and γ-band peak relative power and α-band peak latency of the components in clusters 5, 11, 13, and 20) and the participant characteristics of age, full scale IQ, CARS score, or SCQ score. In the ASD group there was a significant relationship between CARS score and P1 latency [averaged over stimulus spatial frequency) $r(17) = -.67$, $p <$ .01]. No other relationships were significant.

Discussion

The aim of this study was to investigate the cortical dynamics associated with visual perception in individuals with ASD. The initial ERP analysis indicated that latency to peak was reduced in the participants with ASD (Figure 2B). However, as is illustrated in Figure 3, after decomposing the scalp EEG into maximally independent components, (at least) three clusters of independent components were identified that contributed to the ERP elicited by simple visual stimuli. We categorized these clusters as follows:

1. Components located in or near striate and extrastriate cortex. These components showed stimulus-induced increases in spectral power approximately 100 msec after stimulus onset.
2. Components located in or near the parietal cortex. These components showed stimulus-induced decreases in α- and β-band power approximately 300 msec after stimulus onset.
3. Components located in or near the left cingulate gyrus that showed weaker but significant increases in low α-band power approximately 300 msec after stimulus onset.

By comparing the spectral properties of these components across groups, we found differences in the ASD group compared with the TD group in some but not all of these clusters. Specifically, there were no group differences in the components showing α and β desynchronization located in the parietal cortex (Supplement 4), suggesting that the release of inhibition associated with attentional demands (29) does not differ between the two groups. However the induced low α-band power increase in the components located in or near the left cingulate gyrus was significantly stronger in the participants with ASD (Figure 5). Furthermore, in those components located in or near the striate and extra-striate cortex, stimulus spatial frequency exerted a smaller effect on α- and γ-band power in the ASD group (Figure 4A), and latency of the α-band power peak was shorter in the participants with ASD (Figure 4B).

Increased low-α power in the components located in or near the left cingulate gyrus (cluster 4) could reflect different strategies employed during the task in the participants with ASD, because the anterior cingulate provides top-down control of attention (30). A previous report has shown that increased α-band power in an independent component localized in or near the cingulate gyrus was related to drowsiness during a continuous compensatory tracking task (31), and α-band power is negatively correlated with glucose metabolism (measured with positron emission tomography) in the cingulate gyrus (32). Notably, a recent functional MRI study has reported reduced activation of the left anterior cingulate cortex during novelty detection in children with autism (33). However, our definition of the frequency band of the components of cluster 4 should be treated with caution. As the spectrogram in Figure 3A shows, the power increase in cluster 4 was in the lower range of α-band power. Time/frequency computations on longer epochs than were possible here (which would enable computation of lower frequency power changes) are necessary to confirm whether the induced power in cluster 4 is most accurately described as low-α or high-θ.

In the components located in or near striate or extrastriate cortex, spatial frequency affected the induced α- and γ-band power increases less in the ASD group than in the TD group, indicating less specialization within neural networks recruited during visual perception in the ASD group. This finding mirrors previous data illustrating that face-orientation does not modulate the size of induced γ-band power in individuals with ASD (34). In both this and the current study, individuals with ASD showed an increase in induced γ band power relative to mean baseline power, commensurate with perception of the stimulus, but the effect of stimulus characteristics (upright vs. inverted faces or high vs. low spatial frequency Gabor patches) on γ-band power was smaller in the ASD group. γ-band power has been described as the neural signature of perceptual binding (35); therefore reduced selectivity in neural networks recruited during visual perception in ASD might suggest impairment in perceptual binding.

Figures 2B, 2C, and 4A indicate a trend for larger group differences after presentation of high spatial frequency compared with low spatial frequency. Although this could be interpreted as a specific abnormality in networks that are tuned to high spatial frequencies, it could also reflect a more general disturbance of neural synchrony that is evident only when compared against the larger effect induced in the control group. Furthermore, although it is commonly assumed that low and high spatial frequencies are conveyed along the magnocellular and parvocellular visual streams, respectively, this only holds in conditions of low contrast. Given that these stimuli were presented at high contrast (68%), the stimuli presented here will not have isolated specific pathways.

We found, contrary to suggestion in the literature (6), no evidence for hyper-activity in area V1 in individuals with ASD. However, we do find support for "reduced efficiency of neuro-integrative mechanisms operating at a perceptual level in autism" (Bertone *et al.*, 2005, p. 2431). The "complexity-hypothesis" put forward by this group is based on behavioral data showing enhanced perception of simple visual stimuli (first-order parallel gratings) and reduced perception of complex stimuli (second-order parallel gratings) in individuals with ASD (36). This hypothesis proposes that simple visual stimuli can be processed in a single brain area (typically V1), whereas complex stimuli are processed in multiple brain areas, and that reduced functional connectivity in ASD leads to deficient processing of complex but not simple stimuli (5). However, the results of the current study highlight some caveats to this hypothesis. Firstly, as is shown in our data (Figure 3) and has been reported elsewhere (27), the onset of even a simple visual stimulus perturbs the activity of a widespread network including sensory, parietal, and limbic areas. Secondly, we find evidence of disruptions in neural integration after presentation of stimuli that would be classified as "simple" by the complexity hypothesis. In conclusion, we report evidence of neurophysiological abnormality in ASD during visual processing of simple visual stimuli. We identified, in addition to increased relative low-α power in the components that were in or near the cingulate gyrus, two seemingly separate differences in the independent components localized in or near the striate or extrastriate cortex in the participants with ASD. Specifically, the stimulus-induced α-band peak occurred sooner, and stimulus spatial frequency modulation of α- and γ-band power was attenuated in the participants with ASD. There was a negative correlation between P1 peak latency and CARS scores in the ASD group, indicating that the participants with higher CARS scores were also the ones with reduced peak latencies. Reduced peak latency might underpin faster reaction time when detecting visual features in ASD, supporting the argument that the origin of so-called enhanced discrimination in this group is perceptual rather than attentional. Furthermore, given that stimulus-induced increases in spectral power indicate increases in the synchrony and size of the neural networks recruited during perceptual processing, reduced modulation of these networks might suggest abnormality in the mechanisms of neural integration in ASD, which in turn might contribute to the disruption in perceptual binding reported in this group (37).

This work was supported by the Bial Foundation, an Economic and Social Research Council Postdoctoral fellowship, and a World University Network travel grant. Dr. Makeig's contribution was supported in part by the Swartz Foundation (Old Field, New York). Additional funding was provided by a Wellcome Trust Value in People award. We would like to thank all the participants and their families, the staff at the Ryegate Centre, Laurence Vigon for helpful discussions of an earlier draft of this work, and Simon Hamilton and Robin Farr for technical assistance with the figures.

The authors reported no biomedical financial interests or potential conflicts of interest.

Supplementary material cited in this article is available online.

1. O'Riordan M, Plaisted K, Driver J, Baron-Cohen S (2001): Superior visual search in autism. *J Exp Psychol Hum Percept Perform* 27:719–730.
2. Shah A, Frith U (1983): An islet of ability in autistic children: A research note. *J Child Psychol Psychiatry* 24:613–620.
3. Milne E, Swettenham J, Hansen P, Campbell R, Jeffries H, Plaisted K (2002): High motion coherence thresholds in children with autism. *J Child Psychol Psychiatry* 43:255–263.
4. Frith U (1989): *Autism: Explaining the Enigma.* Oxford: Blackwell Scientific Publications.
5. Bertone A, Mottron L, Jelenic P, Faubert J (2005): Enhanced and diminished visuo-spatial information processing in autism depends on stimulus complexity. *Brain* 128:2430–2441.
6. Mottron L, Dawson M, Soulieres I, Hubert B, Burack JA (2006): Enhanced perceptual functioning in autism: An update and eight principles of autistic perception. *J Autism Dev Disord* 36:27–43.
7. von Stein A, Sarnthein J (2000): Different frequencies for different scales of cortical inegration: From local gamma to long range alpha/theta synchronization. *Int J Psychophysiol* 38:310–313.
8. Fründ I, Busch NA, Körner U, Schadow J, Herrmann CS (2007): EEG oscillations in the gamma and alpha range respond differently to spatial frequency. *Vision Res* 47:2086–2098.
9. Boeschoten MA, Kenemnas JL, van Engeland H, Kemner C (2007): Abnormal spatial frequency processing in high-functioning children with pervasive developmental disorder (PDD). *Clin Neurophysiol* 118:2076–2088.
10. Onton J, Makeig S (2006): Information-based modeling of event-related brain dynamics. *Prog Brain Res* 159:99–120.
11. Debener S, Makeig S, Delorme A, Engel AK (2005): What is novel in the novelty oddball paradigm? Functional significance of the novelty P3 event-related potential as revealed by independent component analysis. *Cognitive Brain Research* 22:309–321.
12. Fredericksen RE, Bex PJ, Verstraten FAJ (1997): How big is a Gabor patch and why should we care? *J Opt Soc Am A* 14:1–12.
13. American Psychiatric Association (1994): *Diagnostic and Statistical Manual of Mental Disorders, 4th ed.* Washington DC: American Psychiatric Press.
14. Wing L, Leekam SR, Libby SJ, Gould J, Larcombe M (2002): The Diagnostic Interview for Social and Communication Disorders: Background, inter-rater reliability and clinical use. *J Child Psychol Psychiatry* 43:307–325.
15. Wechsler D (1999): *Wechsler Abbreviated Scale of Intelligence.* San Antonio, Texas: The Psychological Corporation.
16. Schopler E, Reichler RJ, Renner BR (1988): *The Childhood Autism Rating Scale.* Los Angeles: Western Psychological Services.
17. Berument SK, Rutter M, Lord C, Pickles A, Bailey A (1999): Autism Screening Questionnaire: Diagnostic validity. *Br J Psychiatry* 175:444–451.
18. Brainard DH (1997): The psychophysics toolbox. *Spat Vis* 10:433–436.
19. Pelli DG (1997): The VideoToolbox software for visual psychophysics: Transforming numbers into movies. *Spat Vis* 10:437–442.
20. Tucker D (1993): Spatial sampling of head electrical fields: The geodesic sensor net. *Electroencephalogr Clin Neurophysiol* 87:154–163.
21. Delorme A, Makeig S (2004): EEGLAB: An open source toolbox for analysis of single-trial EEG dynamics including independent component analysis. *J Neurosci Methods* 134:9–21.
22. Makeig S, Jung T-P, Bell AJ, Ghahremani D, Sejnowski TJ (1997): Blind separation of auditory event-related brain responses into independent components. *Proc Natl Acad Sci U S A* 94:10979–10984.
23. Oostendorp TF, van Oosterom A (1989): Source parameter estimation in inhomogeneous volume conductors of arbitrary shape. *IEEE Trans Biomed Eng* 47:1487–1492.
24. Ellemberg D, Hammarrenger B, Lepore F, Roy MS, Guillemot J-P (2001): Contrast dependency of VEPs as a function of spatial frequency: The parvocellular and magnocellular contributions to human VEPs. *Spat Vis* 15:99–111.
25. Clark VP, Fan S, Hillyard SA (1995): Identification of early visually evoked potential generators by retinotopic and topographic analyses. *Hum Brain Mapp* 2:170–187.
26. Romani A, Callieco R, Tavazzi E, Cosi V (2003): The effects of collinearity and orientation on texture visual evoked potentials. *Clin Neurophysiol* 114:1021–1026.
27. Foxe JJ, Simpson GV (2002): Flow of activation from V1 to frontal cortex in humans. *Exp Brain Res* 142:139–150.
28. Lancaster JL, Woldorff MG, Parsons LM, Liotti M, Freitas CS, Rainey L, *et al.* (2000): Automated Talairach Atlas labels for functional brain mapping. *Hum Brain Mapp* 10:120–131.

29. Michels L, Moazami-Goudarzi M, Jeanmonod D, Sarnthein J (2008): EEG alpha distinguishes between cuneal and precuneal activation in working memory. *Neuroimage* 15:1296–1310.
30. Takarae Y, Minshew NJ, Luna B, Sweeny JA (2007): Atypical involvement of frontostriatal systems during sensori-motor control in autism. *Psychiatry Res* 156:117–127.
31. Huang R-S, Jung T-P, Makeig S (2005): Analyzing event-related brain dynamics in continuous compensatory tracking tasks. *IEEE Eng Med Biol Mag* 6:5750–5753.
32. Oakes TR, Pizzagalli DA, Hendrick AM, Horras KA, Larson CL, Abercrombie HC, *et al.* (2004): Functional coupling of simultaneous electrical and metabolic activity in the human brain. *Hum Brain Mapp* 21:257–270.
33. Gomot M, Bernard FA, Davis MH, Belmonte MK, Ashwin C, Bullmore ET, *et al.* (2006): Change detection in children with autism: An auditory event-related fMRI study. *Neuroimage* 29:475–484.
34. Grice SJ, Spratling MJ, Karmiloff-Smith A, Halit H, Csibra G, de Haan M, *et al.* (2001): Disordered visual processing and oscillatory brain activity in autism and Williams Syndrome. *Neuroreport* 12:2697–2700.
35. Engel AK, Singer W (2001): Temporal binding and the neural correlates of sensory awareness. *Trends Cogn Sci* 5:16–25.
36. Bertone A, Mottron L, Jelenic P, Faubert J (2003): Motion perception in autism: A "Complex" issue. *J Cogn Neurosci* 15:1–8.
37. Brock J, Brown C, Boucher J, Rippon G (2002): The temporal binding deficit hypothesis of autism. *Dev Psychopathol* 14:209–224.